Ван-дер-Ваальсовы гетероструктуры

Евгений Тихонов

Кафедра физики твердого тела,
Институт физики твердого тела, Черноголовка

ИФТТ РАН
ISSP RAS

29 сентября 2022г.

Энергетические зоны в кристалле

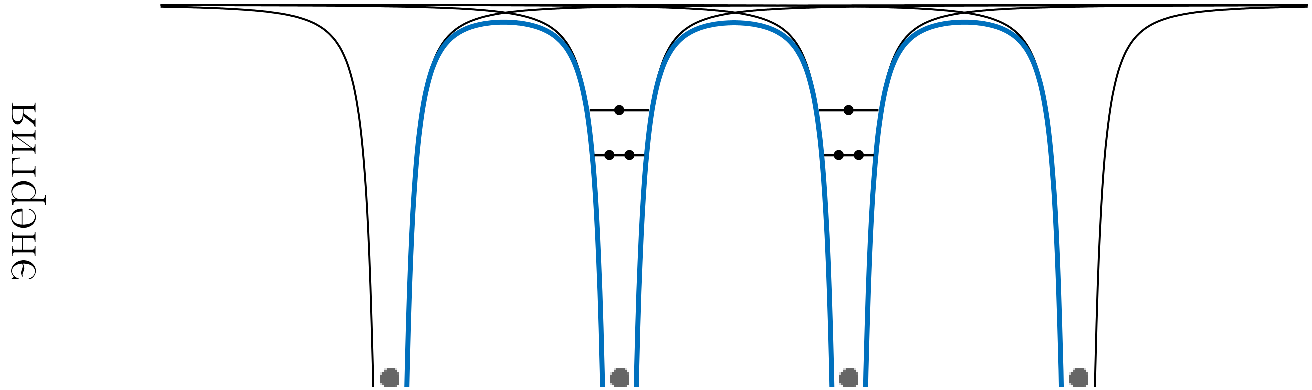

туннелирование
более
эффективно

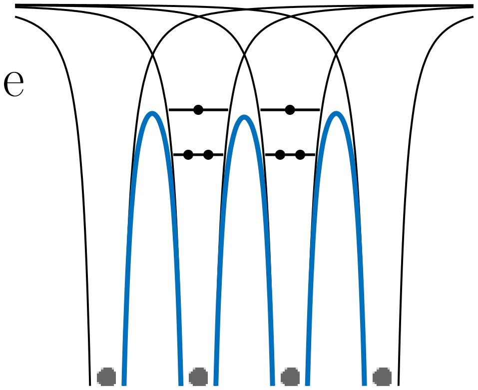

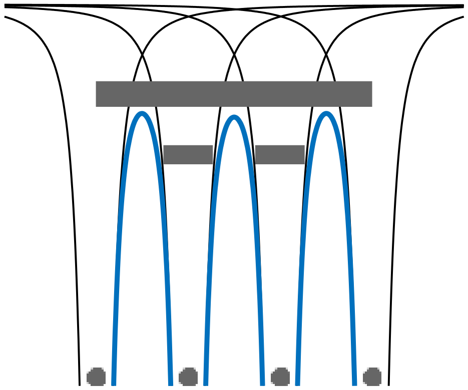

$$\sigma = \frac{ne^2\tau}{m}$$

ширина зоны

$$\tau \sim 10^{-15}\,\text{с} \quad \rightarrow \quad \Delta E \approx \frac{\hbar}{\tau} \sim 10^{-12}\,\text{эрг} \approx 1\,\text{эВ}$$

Проводники и полупроводники: зонная структура и энергия Ферми

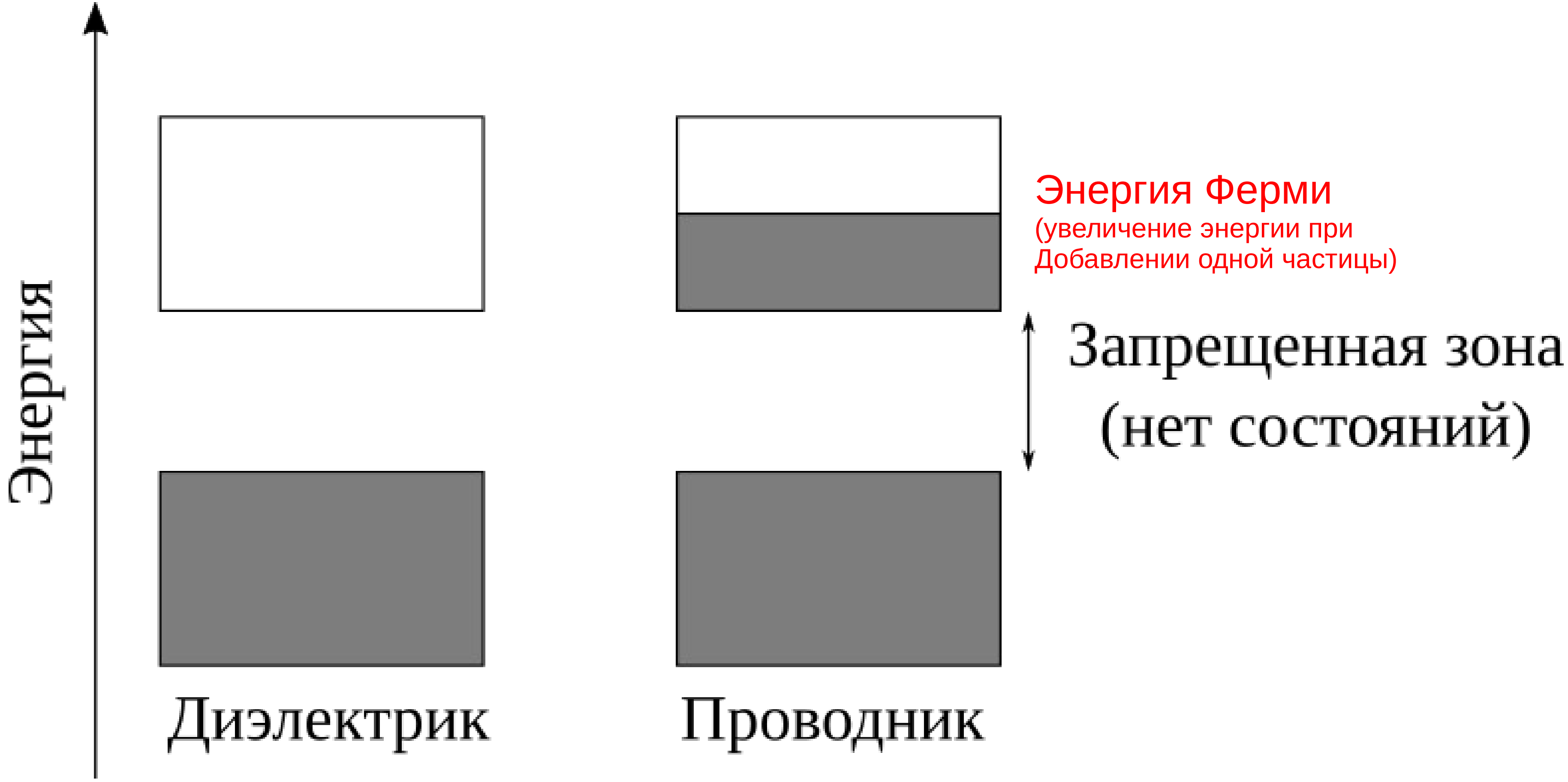

Для транспорта важно где лежит уровень Ферми

Гетероструктуры: инженеринг зон

Нобелевская премия по физике 2000 (Алферов и др.):

за развитие физики полупроводниковых гетероструктур для высокочастотной техники и оптоэлектроники

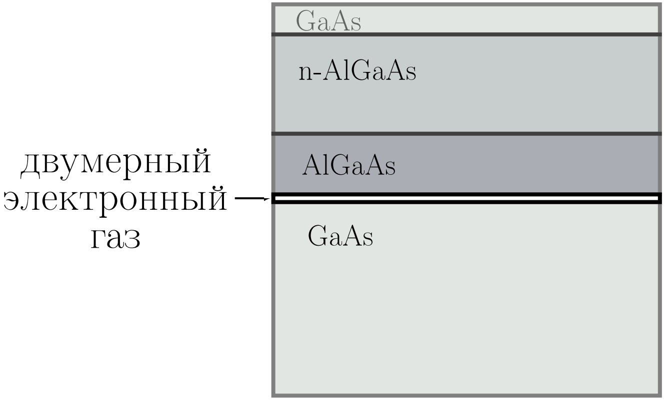

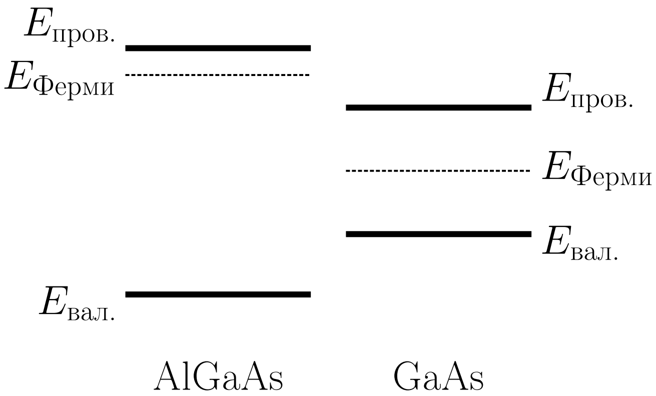

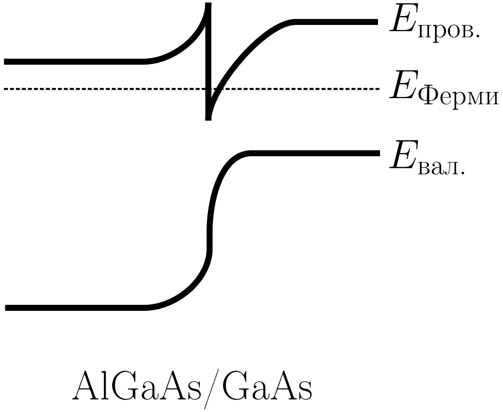

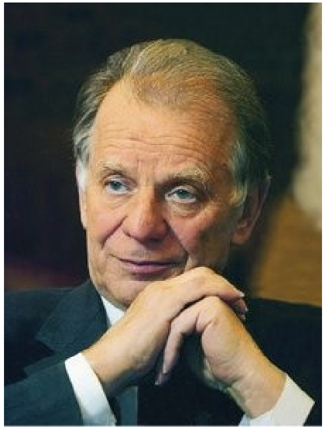

Гетероструктуры: инженеринг зон

Нобелевская премия по физике 2000 (Алферов и др.):

за развитие физики полупроводниковых гетероструктур для высокочастотной техники и оптоэлектроники

На базе гетероструктур создаются быстродействующие опто- и микроэлектронные устройства: лазерные диоды для систем передачи информации в оптоволоконных сетях; гетероструктурные светодиоды и биполярные транзисторы; малошумящие транзисторы с высокой подвижностью электронов (ВПЭТ), применяющиеся в высокочастотных устройствах, в том числе в системах спутникового телевидения; солнечные элементы с гетероструктурами, широко использующиеся для космических и земных программ.

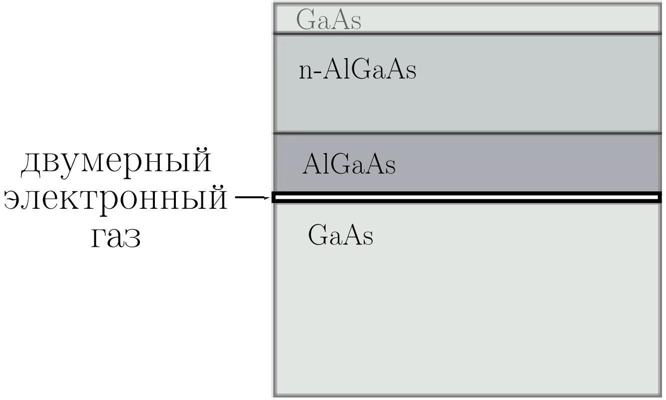

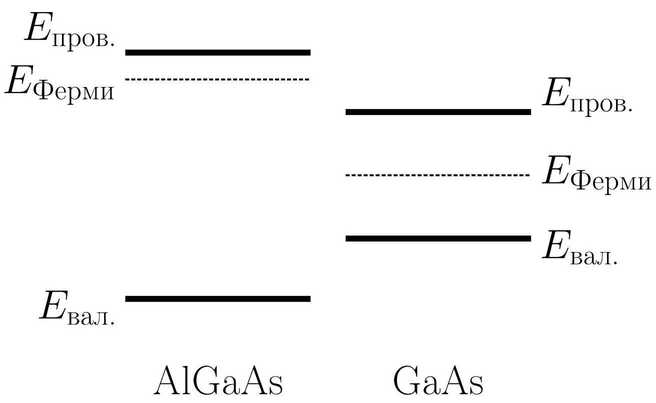

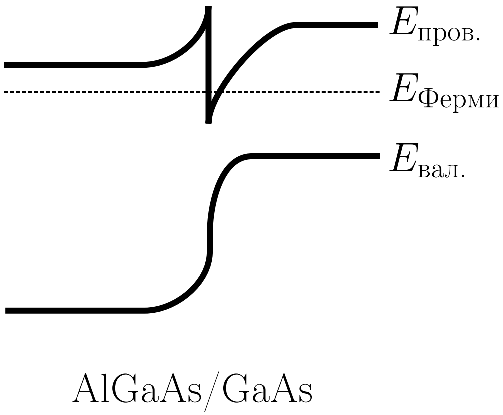

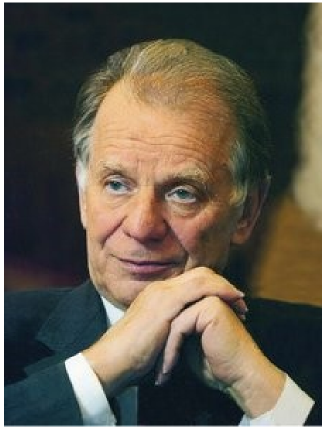

Проводники и полупроводники: зонная структура и энергия Ферми

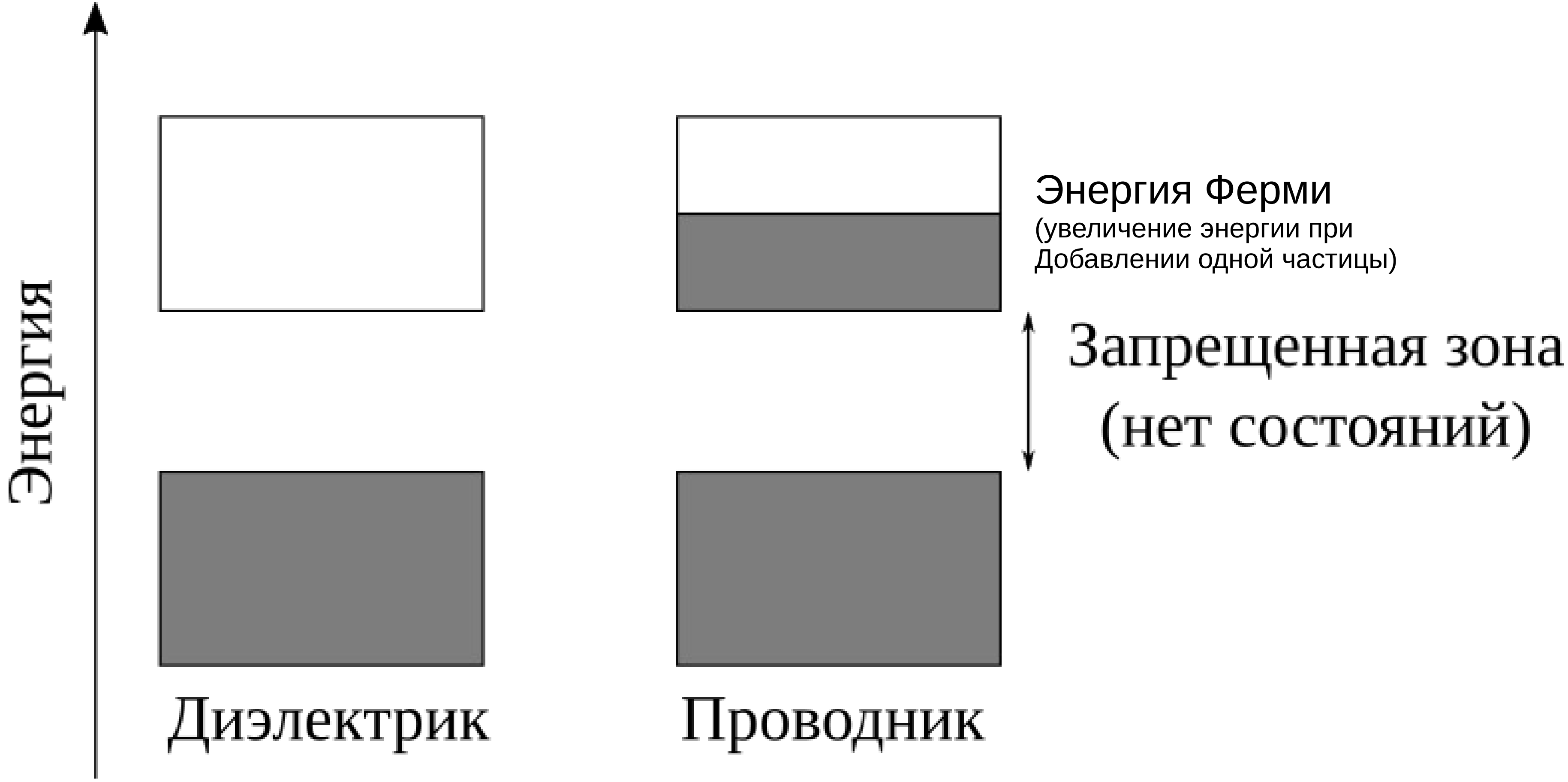

Для транспорта важно где лежит уровень Ферми … и как устроен спектр

Энергетический спектр: как энергия зависит от импульса?

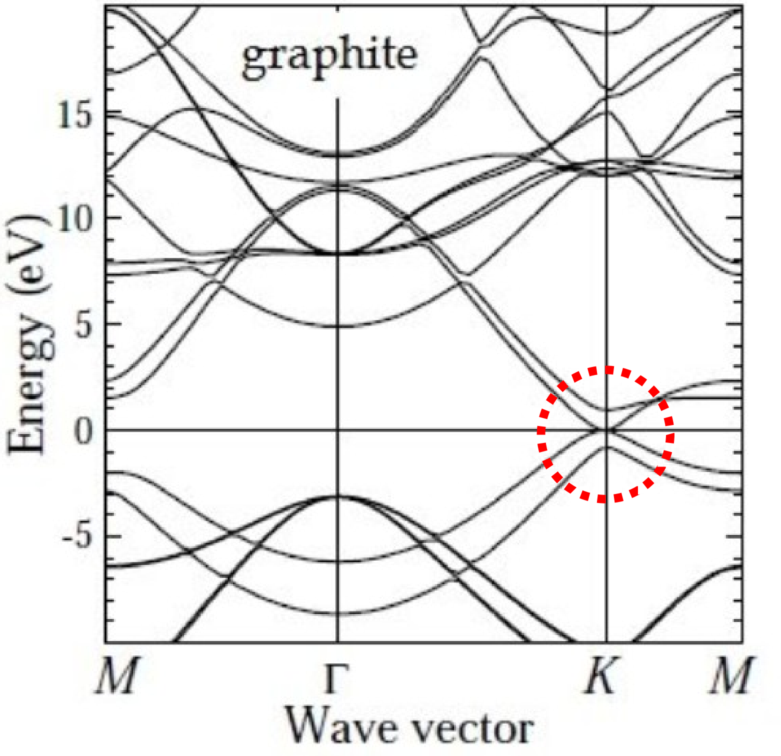

$E \propto k^2$

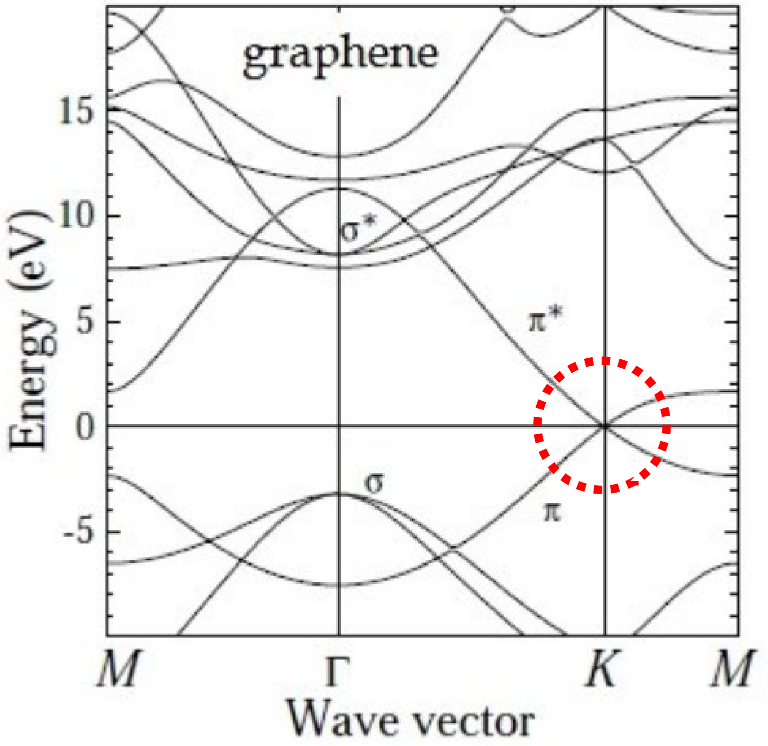

$E \propto k$

релятивистский
спектр

Слоистые материалы

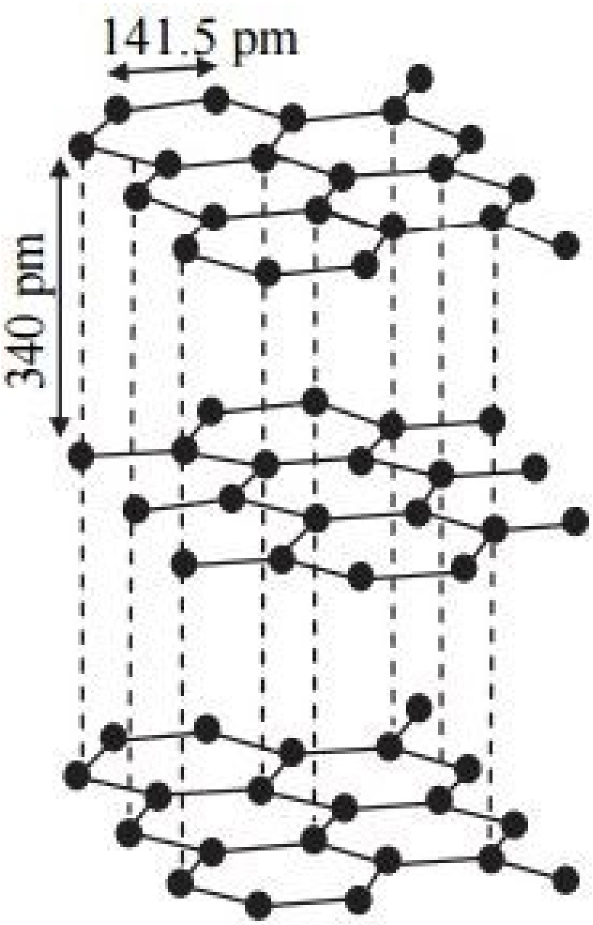

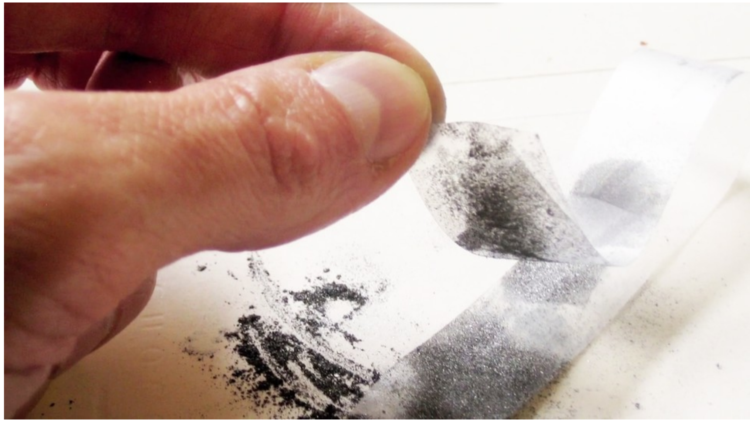

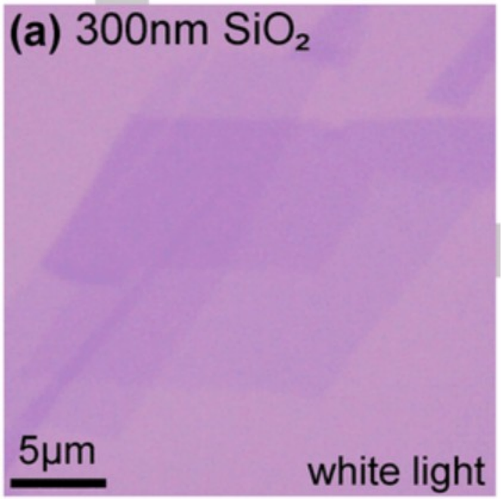

Графен

Нобелевская премия по физике 2010 (Гейм и Новоселов):

за новаторские эксперименты с двумерным материалом графеном

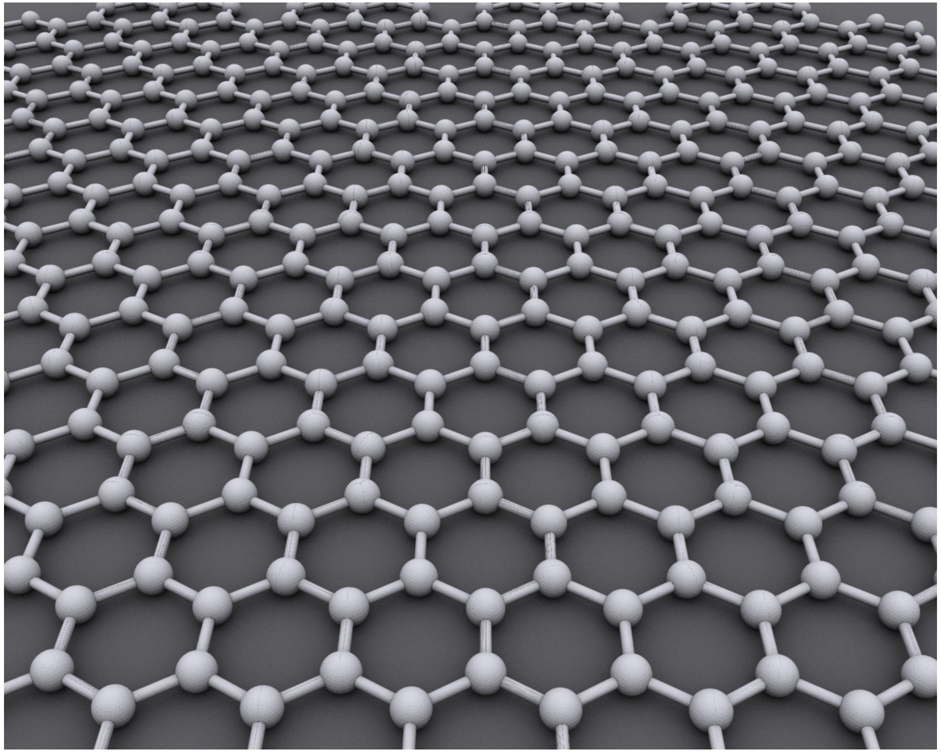

Энергетический спектр: как энергия зависит от импульса?

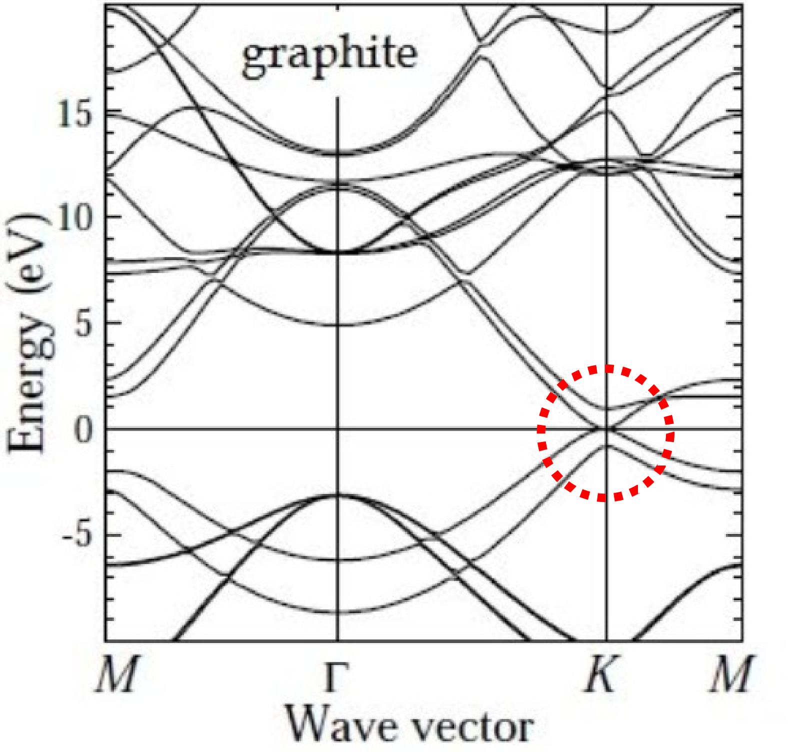

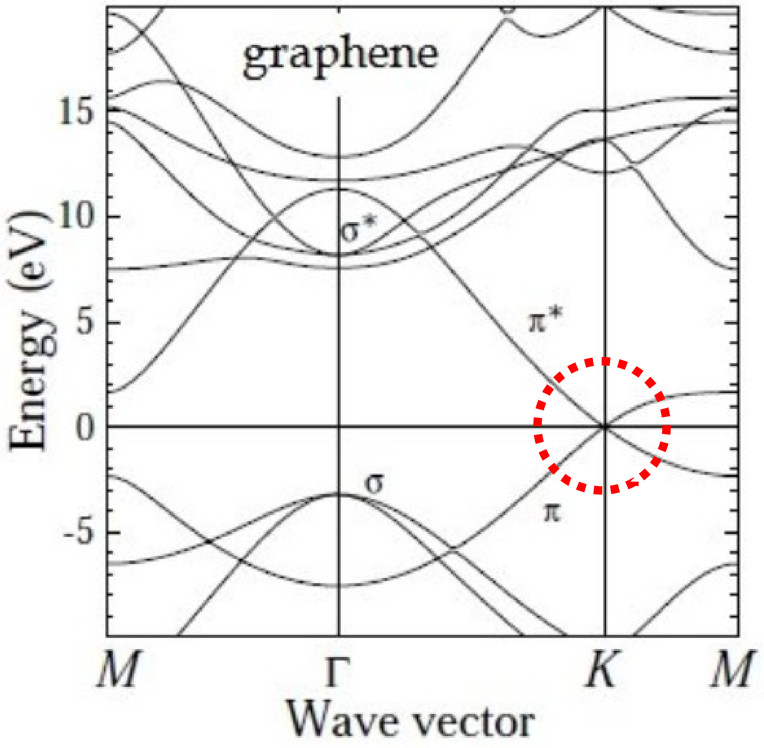

Уровень Ферми

$E \propto k^2$

Для такого спектра концентрация носителей тока $\propto E$ (отсчитывается от 0)

$$\sigma = \frac{ne^2\tau}{m}$$

Как изменить концентрацию носителей?

Графеновый полевой транзистор

Изменение сопротивления поперечным электрическим полем

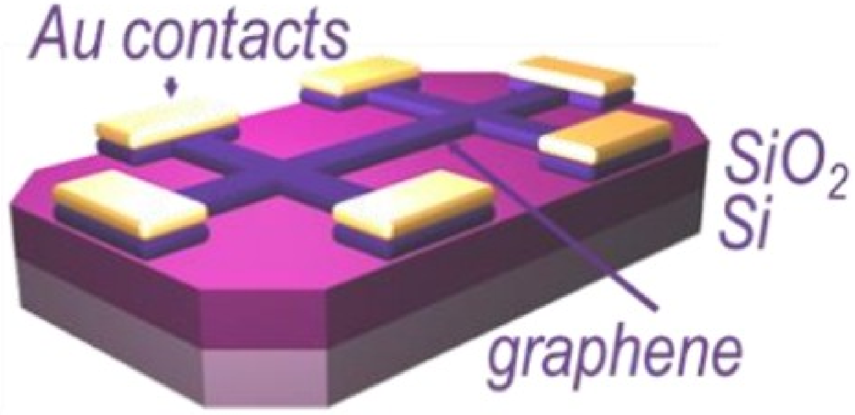

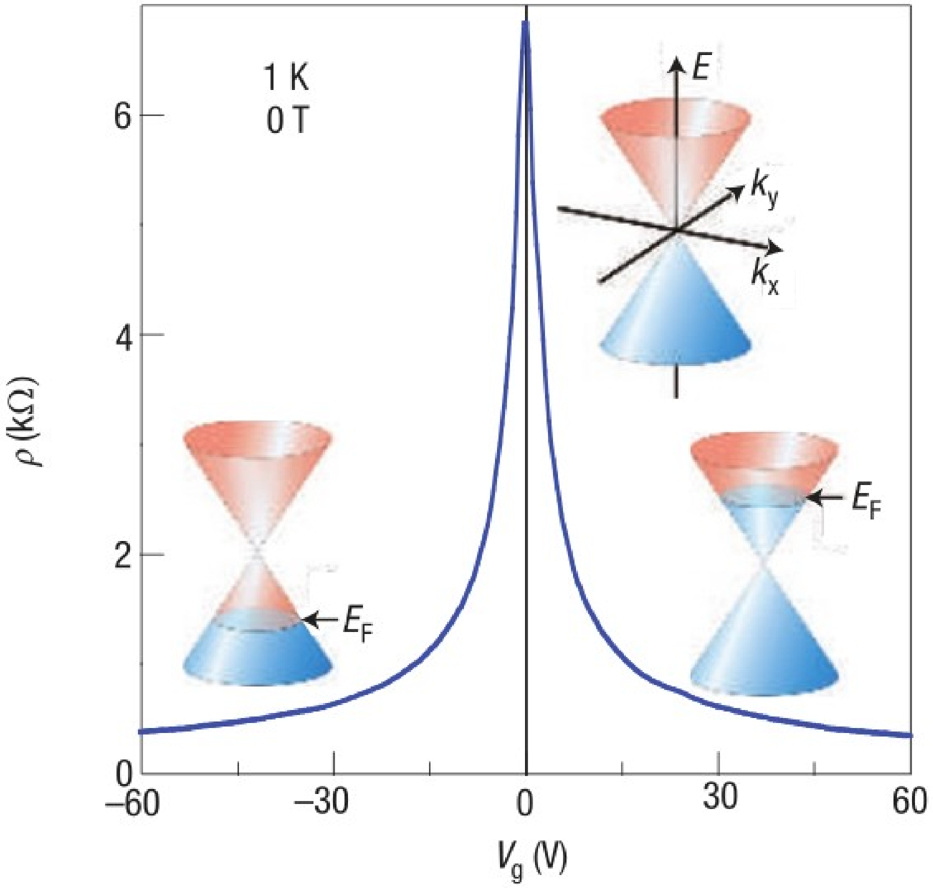

The rise of graphene, Nature Materials 2007

Спектры однослойного и двуслойного графена

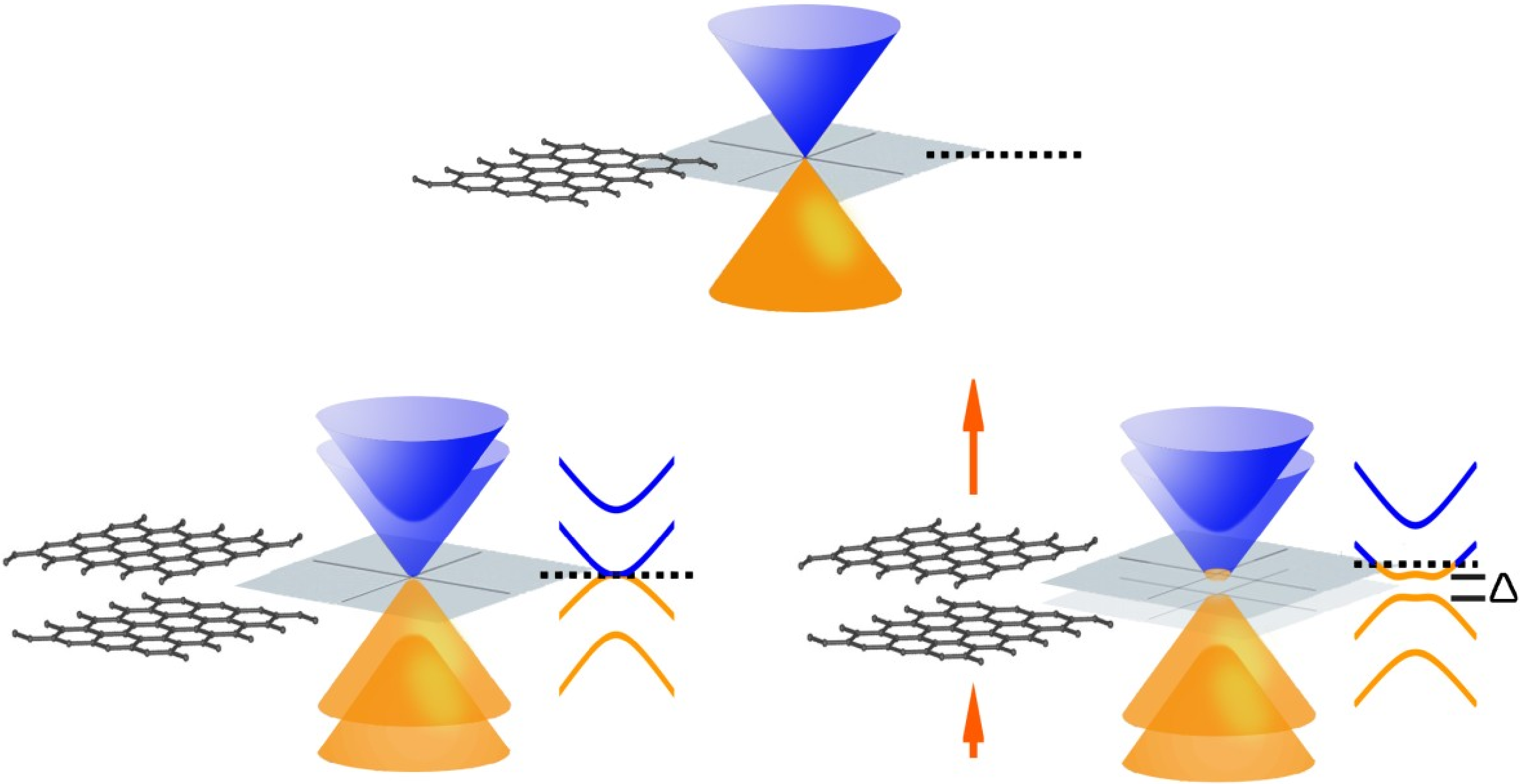

Ван-дер-Ваальсовы гетероструктуры: инжениринг зон-2

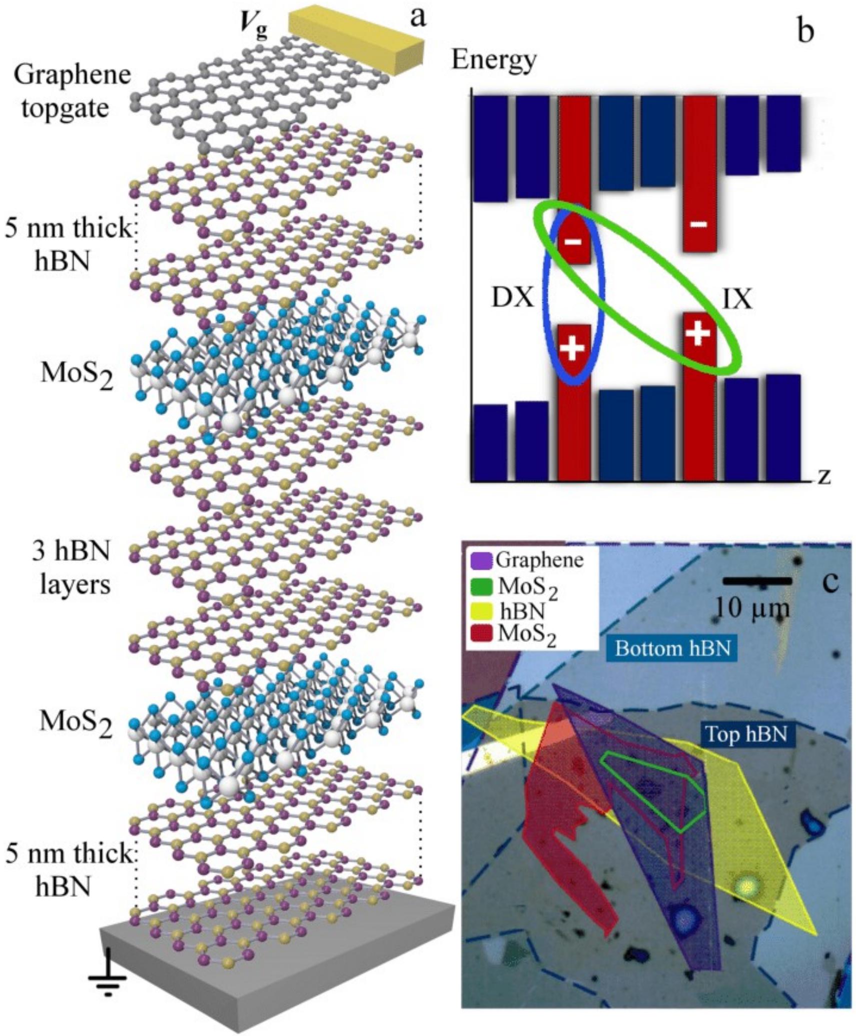

Сверхпроводимость в двуслойном графене: магические углы

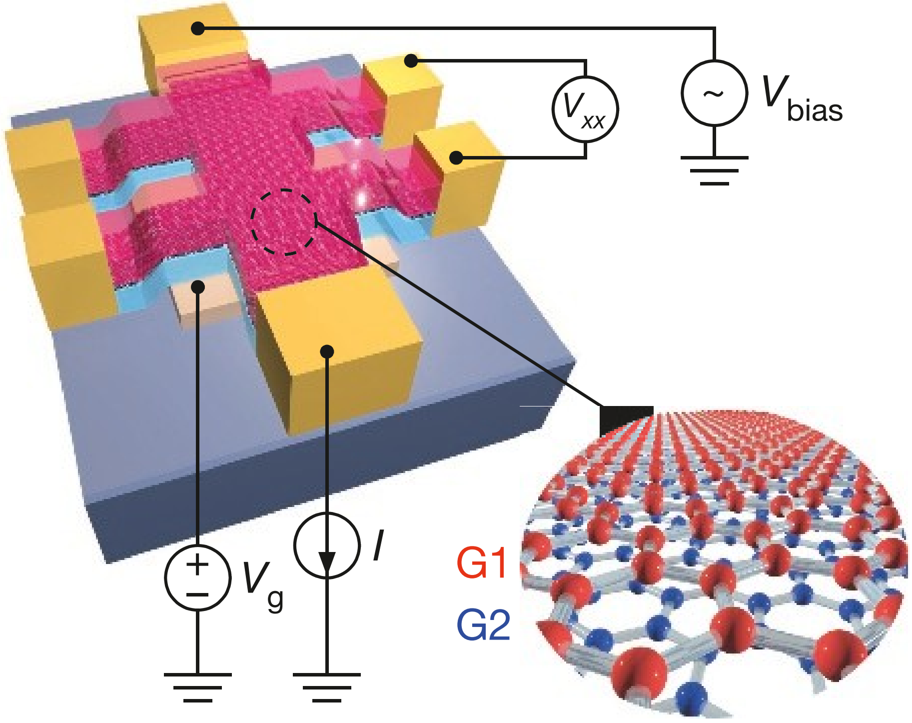

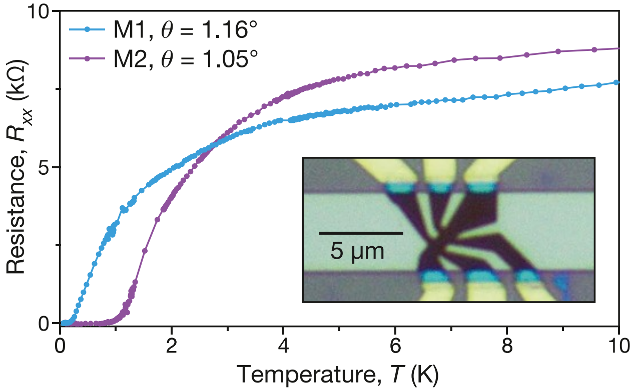

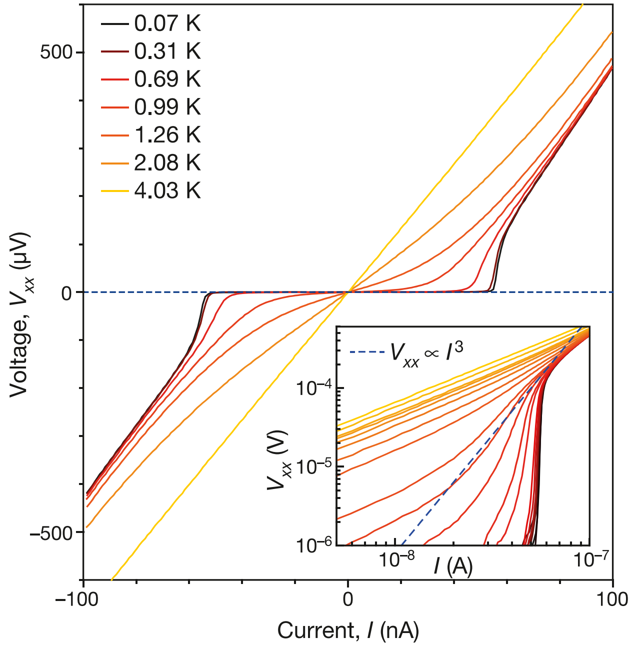

Unconventional superconductivity in magic-angle graphene superlattices, Nature 2018

Муаровый узор

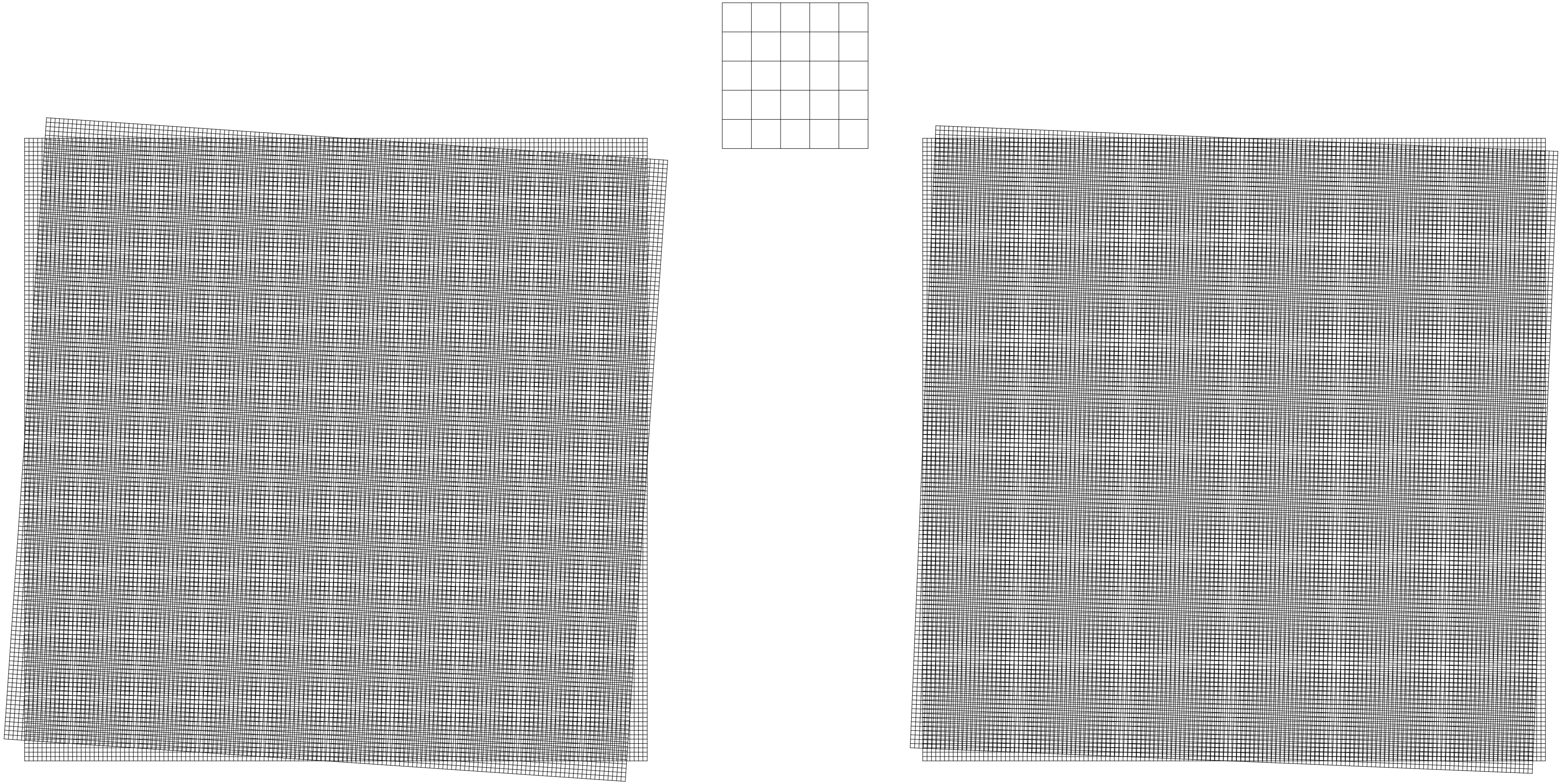

Сверхпроводимость в двуслойном графене: магические углы

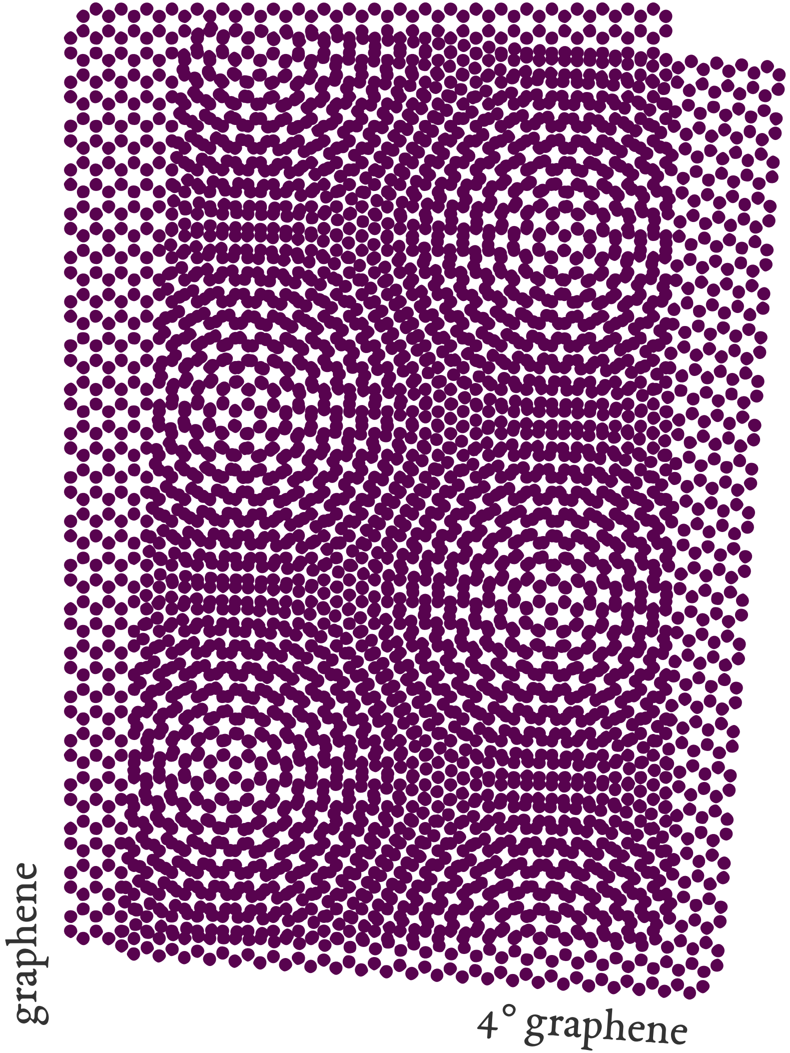

Изменение структуры →

Изменение спектра и всех

связанных с электронами свойств!

Wikipedia: Moire pattern

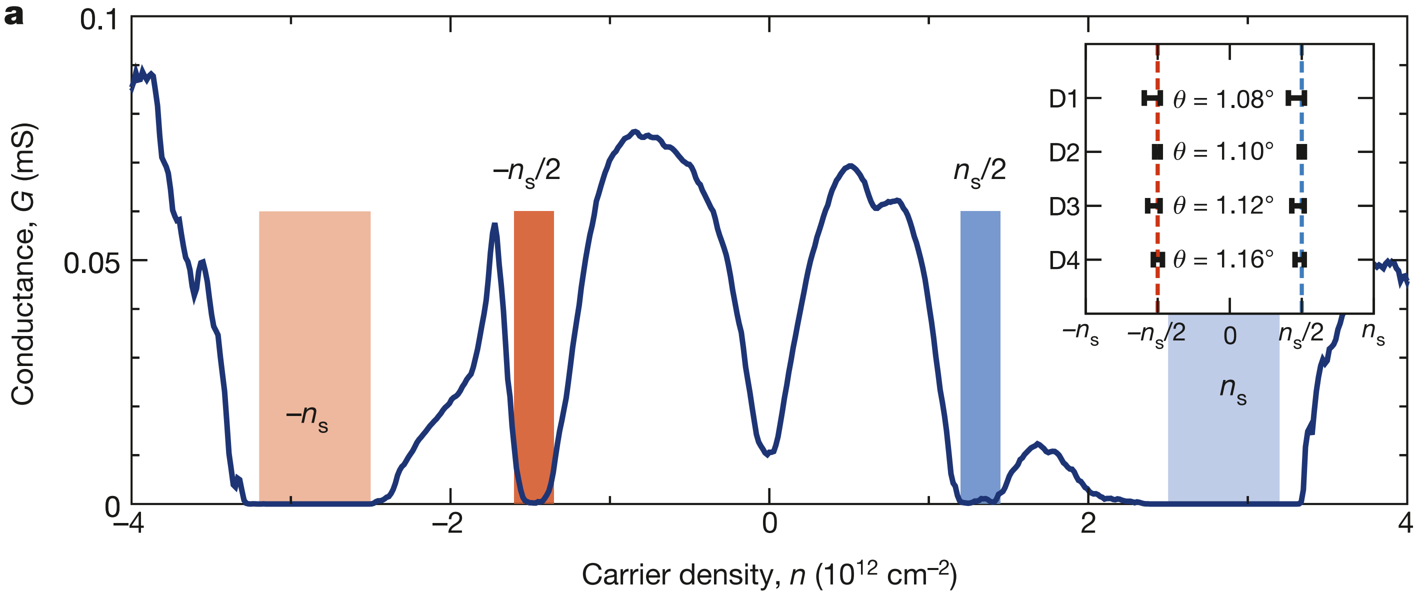

Figure 2 | Half-filling insulating states in magic-angle TBG. a, Measured conductance G of magic-angle TBG device D1 with $\theta = 1.08°$ and $T = 0.3$ K. The Dirac point is located at $n = 0$. The lighter-shaded regions are superlattice gaps at carrier density $n = \pm n_s = \pm 2.7 \times 10^{12}\,\text{cm}^{-2}$. The darker-shaded regions denote half-filling states at $\pm n_s/2$. The inset shows the density locations of half-filling states in the four different devices.

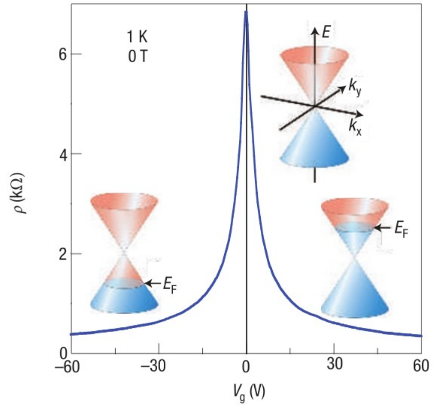

$$\sigma = \frac{ne^2\tau}{m}$$

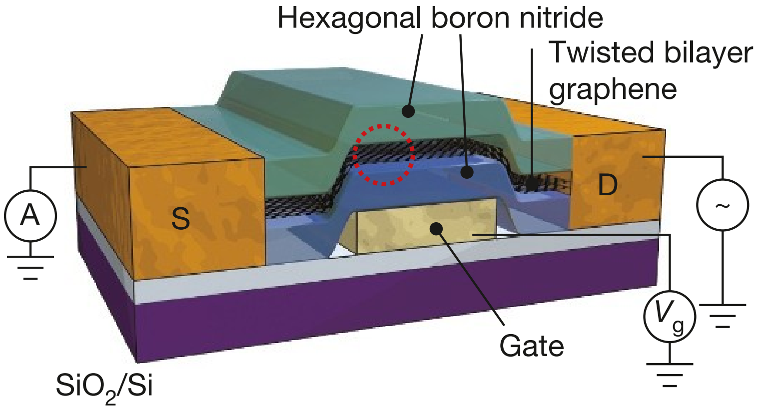

Correlated insulator behaviour at half-filling in magic-angle graphene superlattices, Nature 2018

Что за hBN?

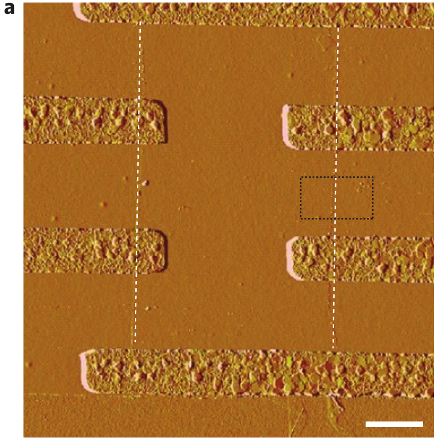

The transferred graphene is free of wrinkles or distortions, consistent with previous reports of similar polymethyl-methacrylate (PMMA)-based transfer techniques[27]. A histogram of the roughness of graphene on h-BN (Fig. 2b) shows it to be indistinguishable from bare h-BN and approximately three times less rough than SiO_2. We conclude that the graphene membrane conforms to the atomically flat h-BN, consistent with previous reports on both rippled[9] and flat[21] surfaces.

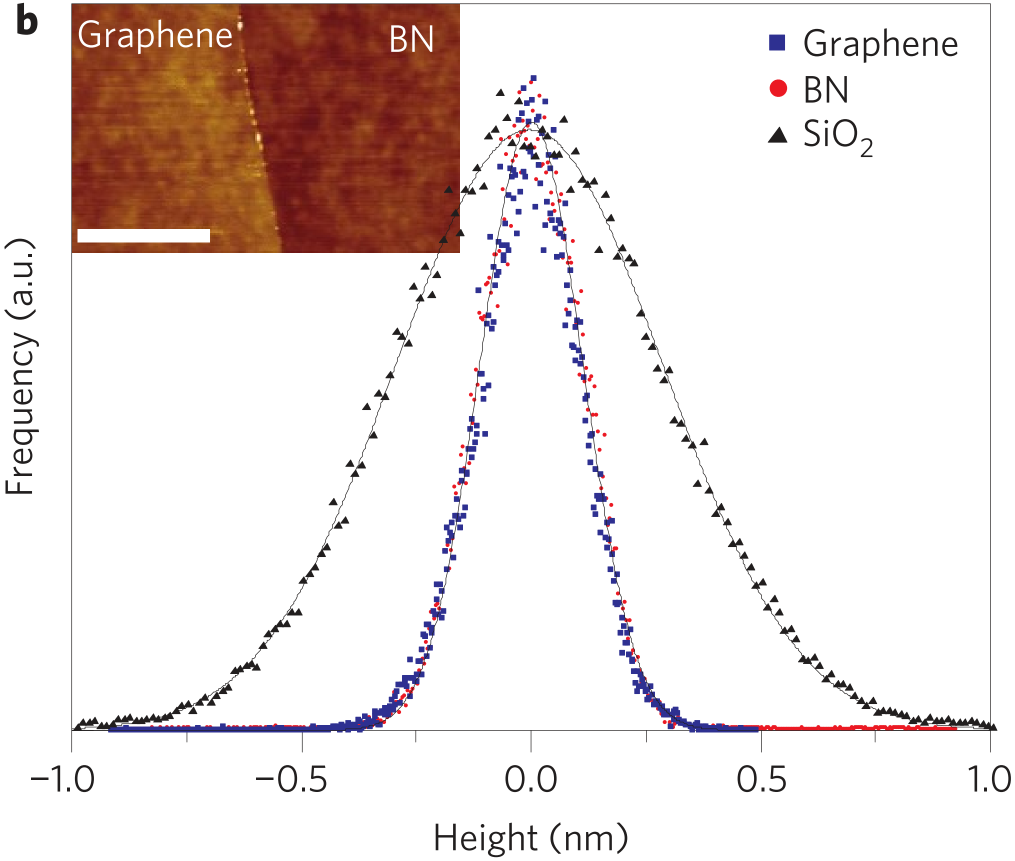

Figure 2 | Atomic force microscopy. a, AFM image of monolayer graphene on BN with electrical leads. White dashed lines indicate the edge of the graphene flake. Scale bar, 2 μm. **b**, Histogram of the height distribution (surface roughness) measured by AFM for SiO_2 (black triangles), h-BN (red circles) and graphene-on-BN (blue squares). Solid lines are Gaussian fits to the distribution. Inset: high-resolution AFM image showing a comparison of graphene and BN surfaces, corresponding to the dashed square in **a**. Scale bar, 0.5 μm.

Boron nitride substrates for high-quality graphene electronics, Nature Nanotechnology 2010

Что за hBN?

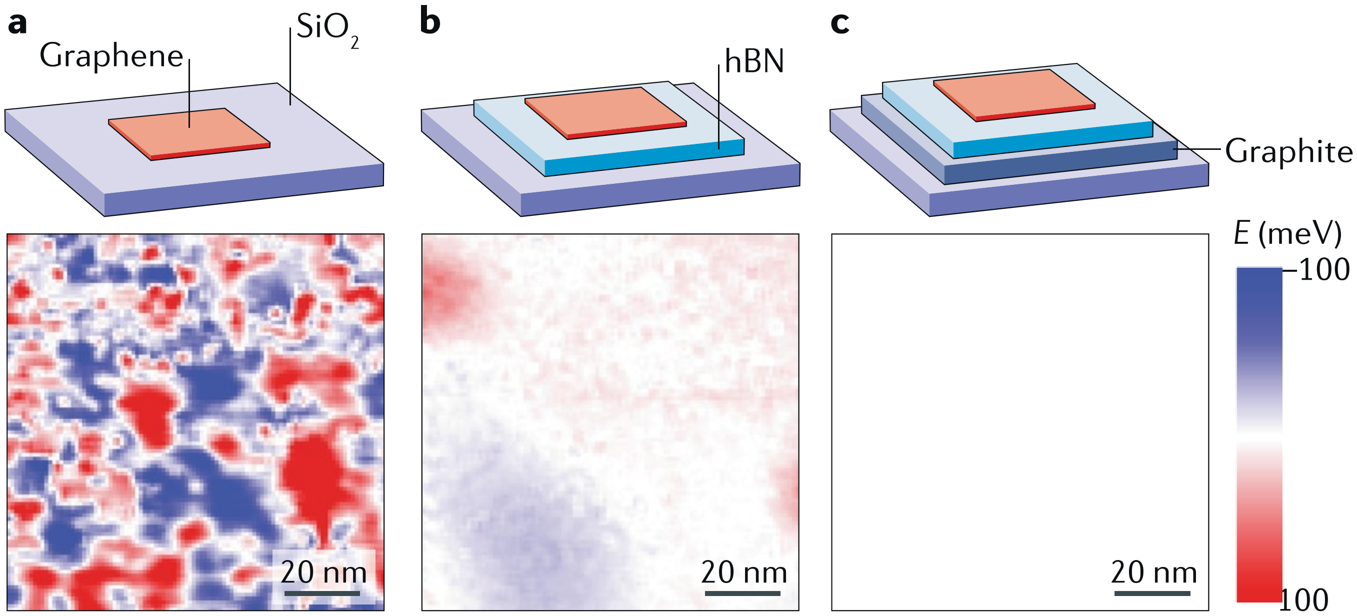

Fig. 2 | **Charge inhomogeneity in graphene devices.** The schematics presented at the top of the figure show the structures of different devices; the images presented at the bottom of the figure show charge fluctuations measured by scanning tunnelling spectroscopy in each device. The experimental images display the tip voltage of the minimum in the differential conductance curve measured at each location, which corresponds to the energy E of the Dirac point. The devices are graphene on SiO$_2$ (panel **a**), graphene on an ~20 nm hexagonal boron nitride (hBN) substrate (panel **b**) and graphene on an ~20 nm hBN substrate with an additional graphite bottom gate (panel **c**).

van der Waals heterostructures combining graphene and hexagonal boron nitride, Nature Reviews | Physics 2019

Как собрать?

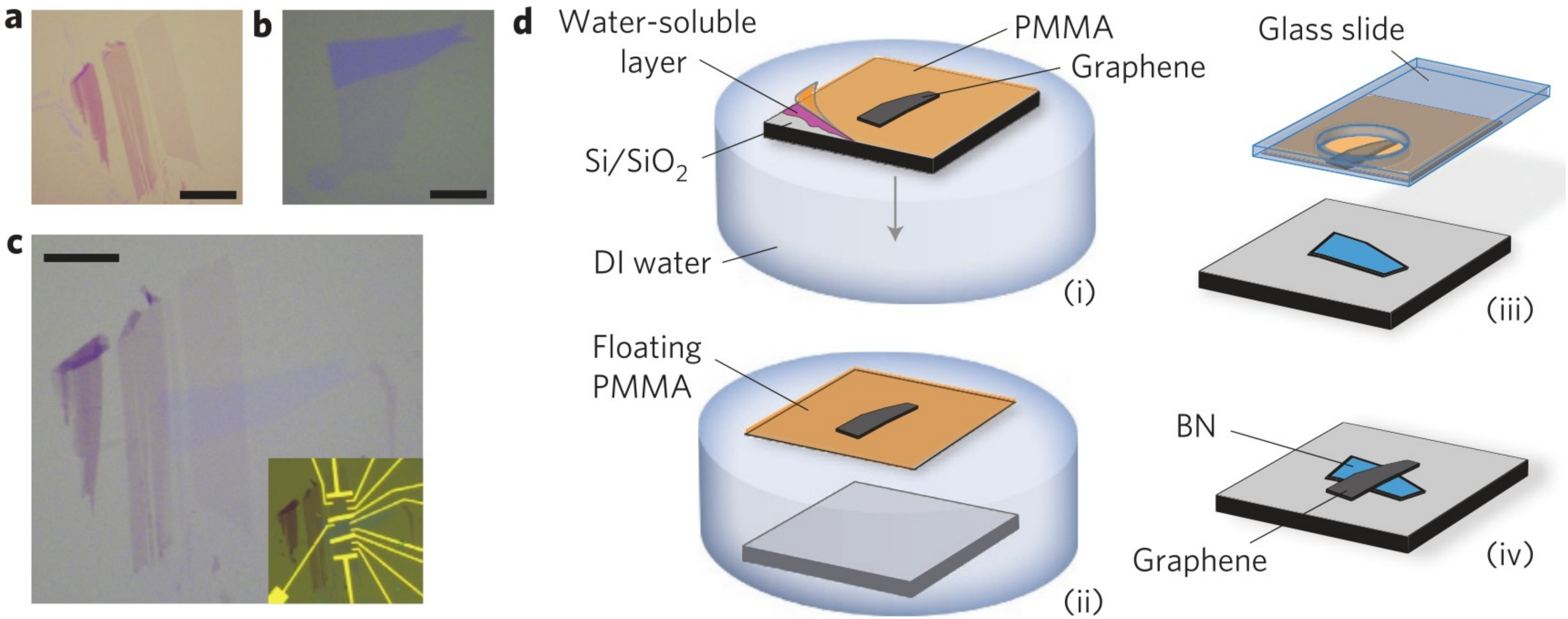

a–**c**, Optical images of graphene (**a**) and h-BN (**b**) before and after (**c**) transfer. Scale bars, 10 μm.

Once transferred, the PMMA was dissolved in acetone (Fig. 1d(iv)). Electrical leads were deposited using standard electron beam lithography, after which all samples were annealed in flowing H_2/Ar gas at 340 °C for 3.5 h to remove resist residues.

Boron nitride substrates for high-quality graphene electronics, Nature Nanotechnology 2010

Как собрать?

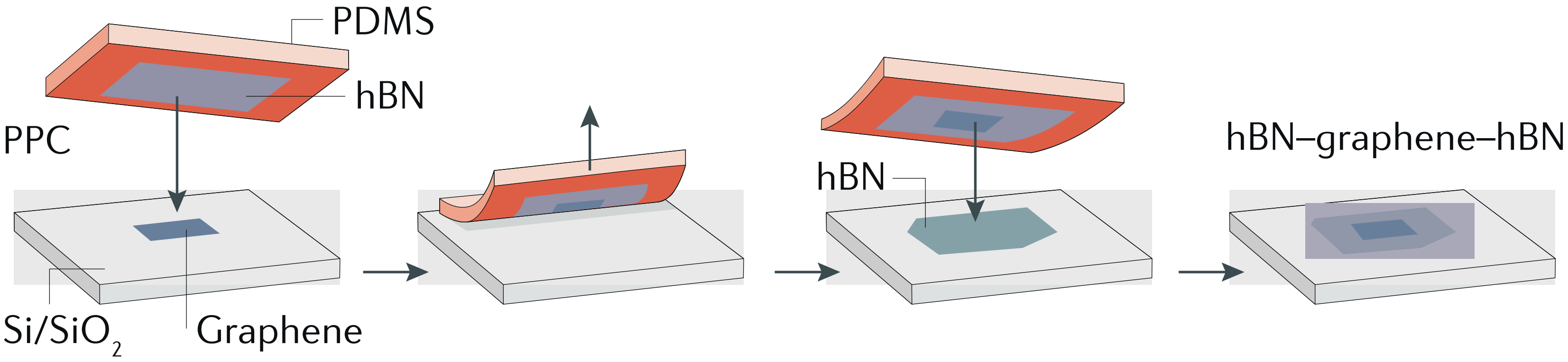

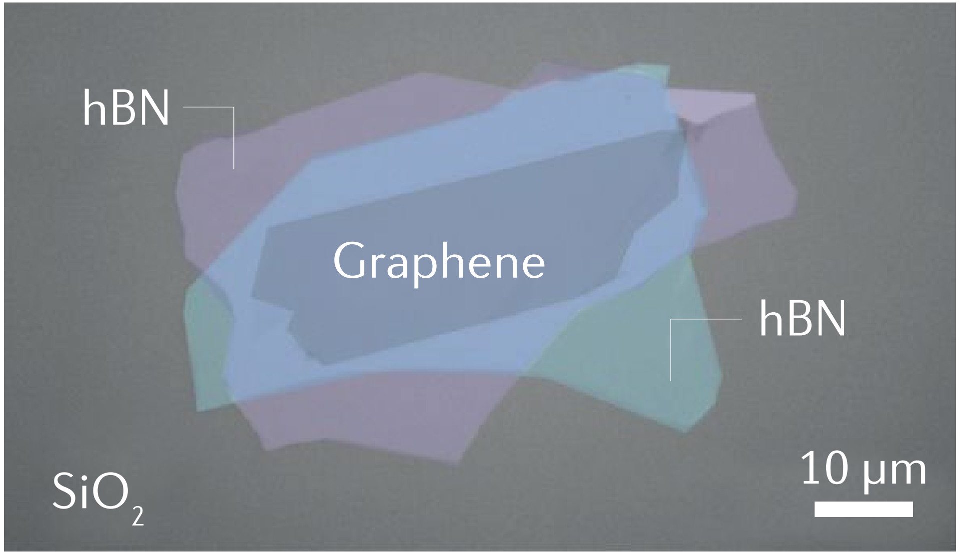

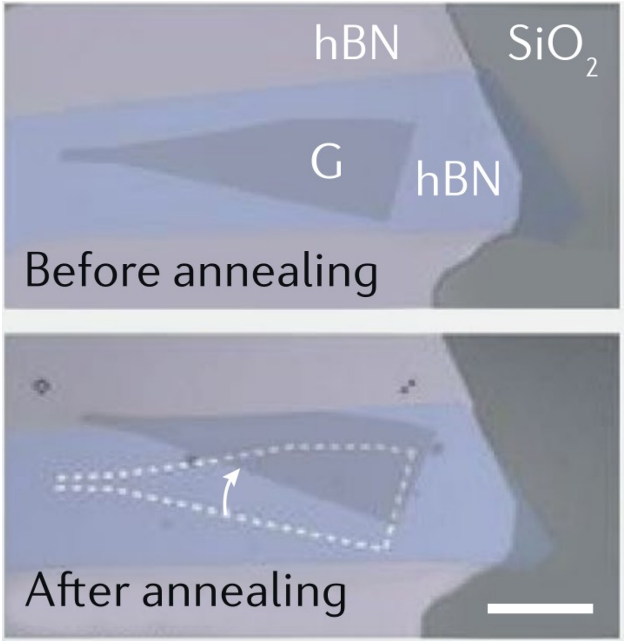

van der Waals heterostructures combining graphene and hexagonal boron nitride, Nature Reviews | Physics 2019

Муар графена на hBN

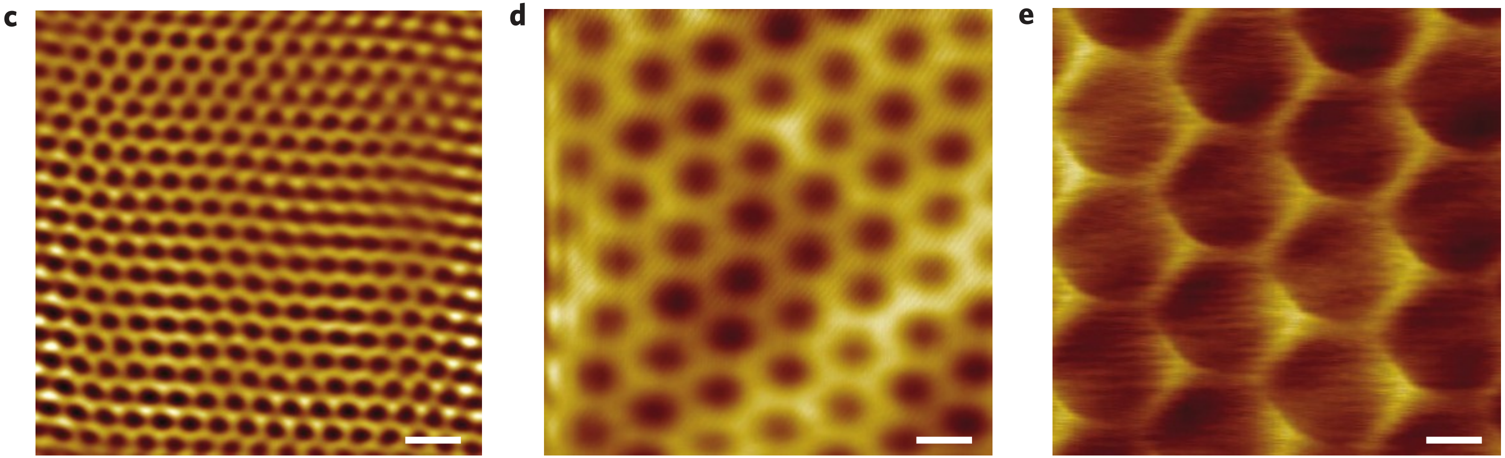

Figure 1 | Graphene device schematic and STM moiré images. a, Schematic of the measurement set-up showing the STM tip and an optical microscope image of one of the measured samples. **b**, Superlattice wavelength (black) and rotation (red) as a function of the angle between the graphene and hBN lattices. **c**–**e**, STM topography images showing 2.4 nm (**c**), 6.0 nm (**d**) and 11.5 nm (**e**) moiré patterns. Typical imaging parameters were sample voltages between 0.3 V and 0.5 V and tunnel currents between 100 pA and 150 pA. The scale bars in all images are 5 nm.

Emergence of superlattice Dirac points in graphene on hexagonal boron nitride, Nature Physics 2012

Как отжиг влияет на транспорт заряда

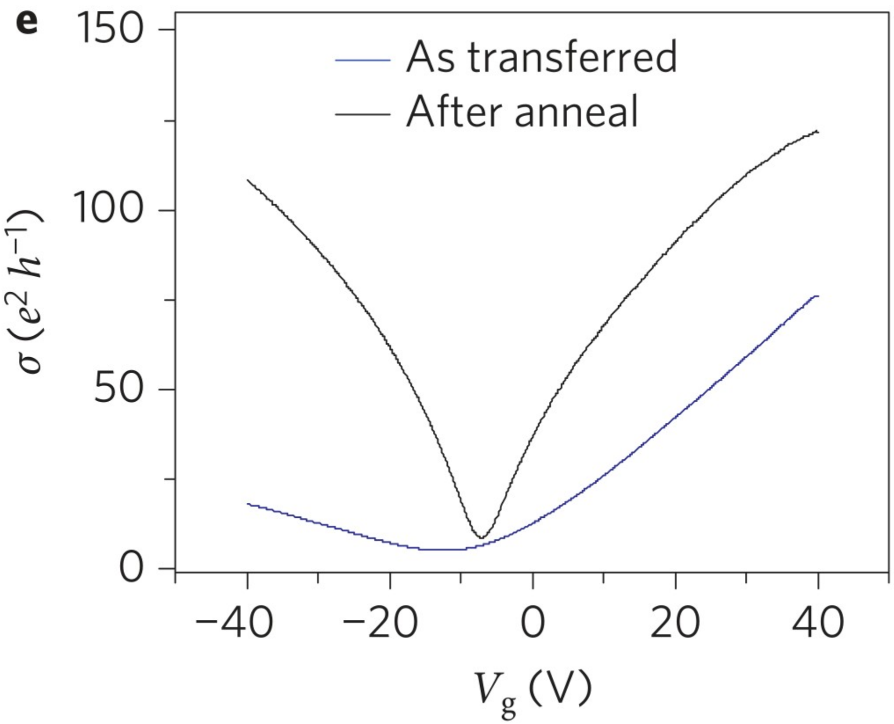

The chemical reactivity of our graphene-on-h-BN heterostructures appears to be markedly different from that of graphene-on-SiO_2. Figure 3e shows the room-temperature conductivity of a typical monolayer graphene layer before and after annealing in a H_2/Ar flow at 340 °C for 3.5 h (see Methods). Annealing substantially enhances the carrier mobility while leaving the position of the charge neutrality point virtually unchanged. The low mobility immediately post-transfer may be due to neutral transfer residues and/or local strains that are relaxed upon heating. The lack of doping after heating in H_2/Ar is in stark contrast to SiO_2-supported devices, where heat treatment typically results in heavy doping of the graphene, often more than $5 \times 10^{12}\,\mathrm{cm}^{-2}$, after re-exposure to air. The mechanism responsible for this different behaviour remains unclear, because features of both the substrate (for example, surface chemistry) and the graphene (for example, roughness) may play a role.

Boron nitride substrates for high-quality graphene electronics, Nature Nanotechnology 2010

Однослойный WTe_2 – топологический изолятор

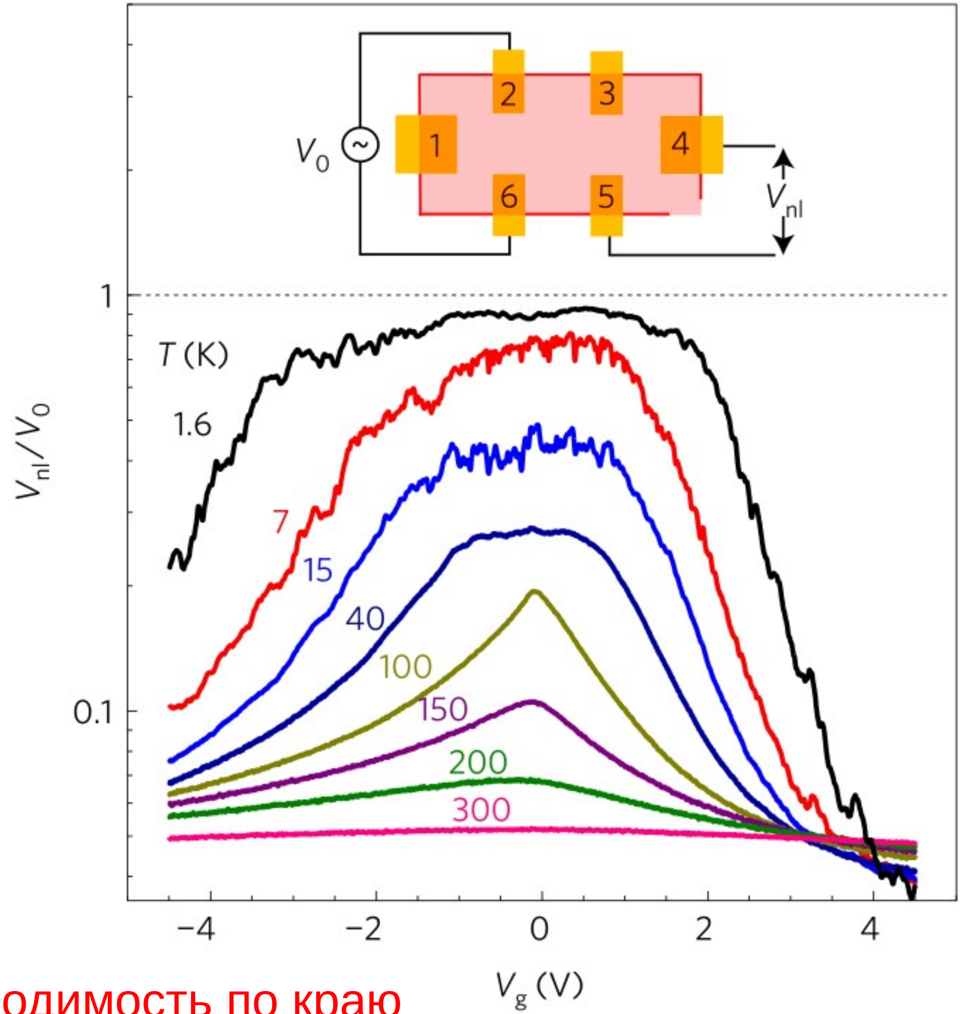

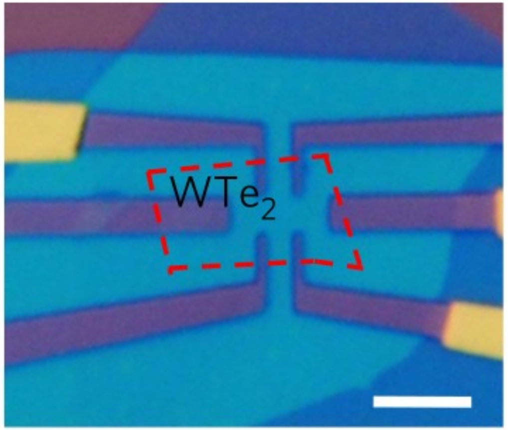

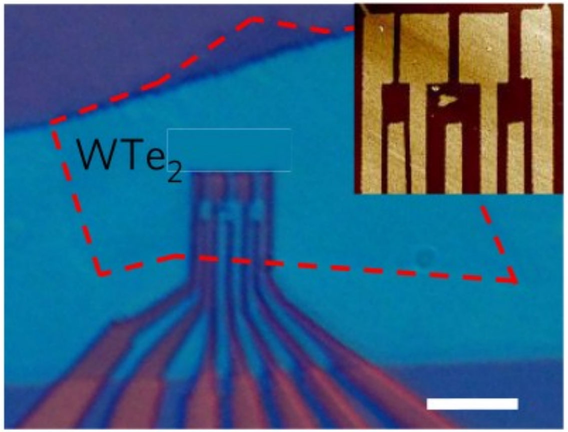

Проводимость по краю
В объеме – диэлектрик!

Edge conduction in monolayer WTe2, Nature Physics 2017

Сверхпроводимость в однослойном WTe_2

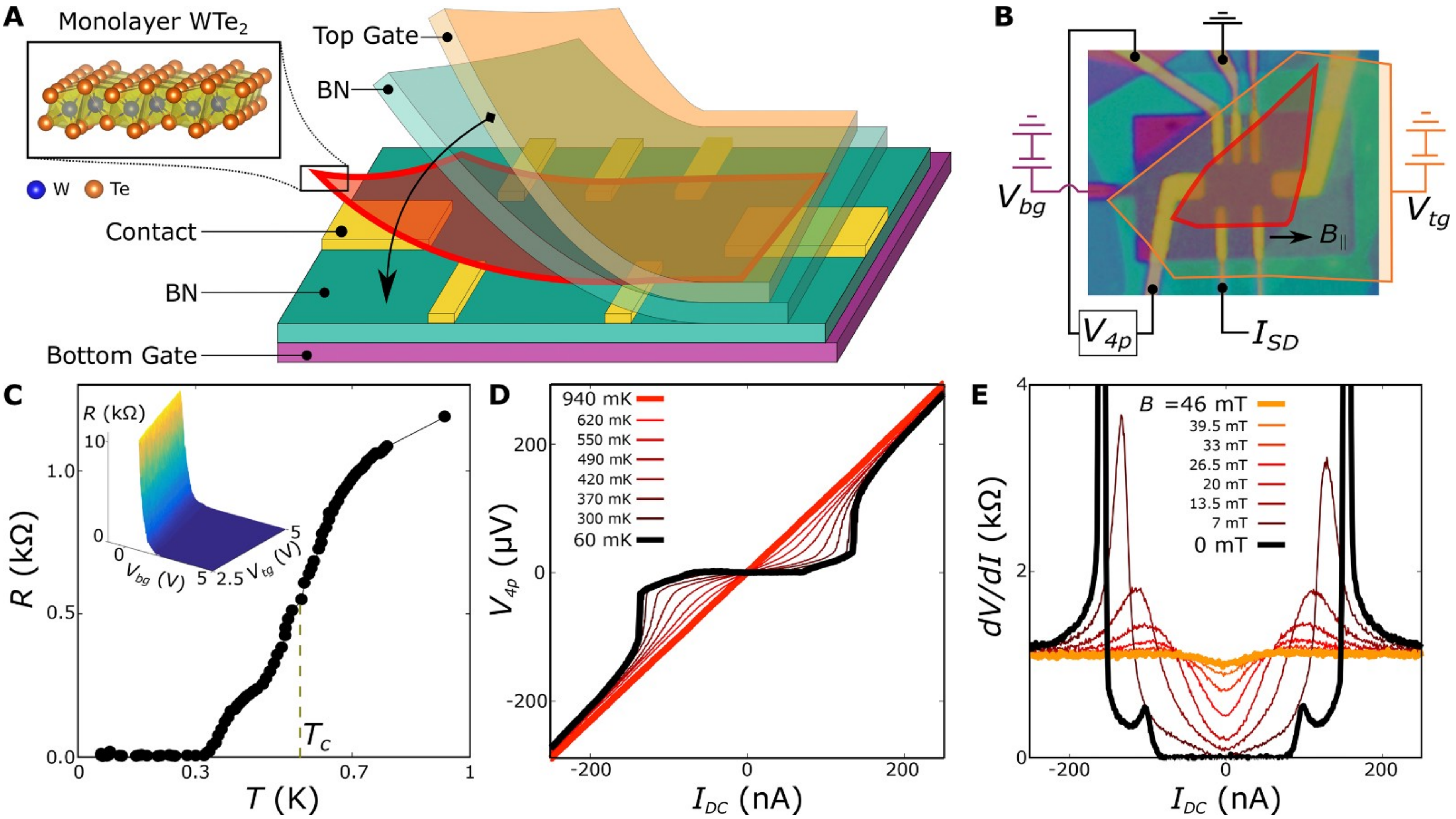

Electrically tunable low-density superconductivity in a monolayer topological insulator, Science 2018

Как сделать образец? :)

1. Creation of Gate Electrodes
   d. Deposit Cr(3nm)/PdAu(30nm) in a thermal evaporator.

   f. Heat clean at 300C for 3+ hours in forming gas (H_2 + Ar).
2. Transfer of bottom hBN
   a. Exfoliate hBN onto cleaned Si/SiO_2 wafer.
   b. Heat clean at 400C for 3+ hours in forming gas.
   c. AFM to ensure cleanliness of the flake.
   d. Pick up and transfer the flake onto the gates via standard dry transfer techniques using a polycarbonate/PDMS stamp.
   e. Remove the transfer polymer with chloroform.
   f. Heat clean at 300C for 3+ hours in forming gas.

3. Creation of Contact Electrodes
   d. Deposit Ti(3nm)/PdAu(30nm) in a thermal evaporator. The height of the electrodes matches the local gates, to minimize the stressed (not fully encapsulated) region at the vicinity of the inner-most contacts.

Observation of the quantum spin Hall effect up to 100 kelvin in a monolayer crystal, Science 2018